An analytical model to study the frequency response of ultrasonic welding transducers

Amir Yazdian
Tarbiat Modares University
Mohammad Reza Karafi (karafi@modares.ac.ir)
Tarbiat Modares University

Article

Keywords: Transducer, Stiffness, Ultrasonic welding, Analytical model, Frequency Response

Posted Date: June 21st, 2022

DOI: https://doi.org/10.21203/rs.3.rs-1737951/v1

An analytical model to study the frequency response of ultrasonic welding transducers

Amir Yazdian[1], Mohammad Reza Karafi[2*]
1,2- Faculty of Mechanical engineering, Tarbiat Modares University, Tehran, Iran.
Corresponding author E-mail: karafi@modares.ac.ir

Abstract

This paper develops an analytical 3D model of ultrasonic welding transducers. The presented model investigates the effects of the workpiece's stiffness and material properties on transducers' frequency response and mode shape. Longitudinal and lateral vibration is taken into account in the model. In order to analyze the forced vibration of the transducer, the effect of piezoelectric and excitation electrical fields are considered. The structural damping is considered as an imaginary Young's modulus. For validation of the model, a transducer, booster, and horn with specific dimensions and physical properties is modeled in ANSYS software. Its resonant frequency is compared with the mathematical model. Then, the system is fabricated for experimental tests. The resonant frequency in the analytical model, simulation, and the experimental test is achieved, 19208 Hz, 19280 Hz, and 19203 Hz, respectively. There is a 0.02% error between the analytical model and the experimental test. The Anti-resonant frequency in the analytical model is 19265 Hz which has a 0.02% error with experiment (19270 Hz). The admittance at a resonant frequency in the analytical model is 0.01755 mS which has a 0.2% error with the experiment (0.0176 mS). The mechanical quality factor of the transducer and its vibration amplitude are calculated by the developed analytical model according to the mechanical properties of components.

Keywords:

Transducer, Stiffness, Ultrasonic welding, Analytical model, Frequency Response

Nomenclature

Symbol	Description	Unit
a_i	The outer diameter of the cylindrical element and piezoelectric	m
b	The inner diameter of the cylindrical element and piezoelectric	m
d_{ij}	Piezoelectric constants	m/V
C	Damping coefficient	Ns/m
D	Electric charge density	C/m^2
D_{31} , D_{33}	Electric charge density due to radial and longitudinal vibrations	C/m^2
E	Modulus of elasticity	N/m^2
E_r , E_z	Apparent modulus of elasticity in radial and longitudinal directions	N/m^2
E', E"	Real young modulus (storage modulus), Imaginary young modulus (loss modulus)	N/m^2
E_3	Electric field along the z-direction	V/m
V_3	Applied voltage to piezoelectric	V

f_r	Resonant frequency	Hz
F	The force	N
I	The total current of piezoelectric	A
I_{31} , I_{33}	Currents of the piezoelectric due to radial and longitudinal vibrations	A
J_0 , J_1	Bessel functions of the first kind	
Y_0 , Y_1	Bessel functions of the second kind	
k_r , k_z	Apparent wave numbers in radial and longitudinal directions	rad/m
K	Spring stiffness	N/m
l_i	Length of the components	m
m	Mass	kg
n	Mechanical coupling coefficient	
N_p	Number of piezoelectric	
Q_m	Mechanical quality factor	
r	The radius of the cylindrical element	m
$\boldsymbol{s_{ij}^E}$	Elastic compliance at constant electric field	m^2/N
tan δ	Dissipation factor	
u_r , u_z	Displacement in radial and longitudinal directions	m
$U_i(z_i)$	Displacement of the components	m
Y_{31} , Y_{33}	Admittance of transducer due to radial and longitudinal vibrations	S
Y_3	Total admittance	S
$\boldsymbol{\varepsilon_{ij}^T}$	The electrical permittivity of piezoelectric at constant stress	C/Vm
ε', ε"	The real and imaginary electrical permittivity of piezoelectric	C/Vm
η	Loss factor	
V	Sound speed	m/s
ξ	Damping ratio	
ρ	Density	kg/m^3
σ	Stress	N/m^2
ω	Angular frequency	rad/s

1. Introduction

Nowadays, ultrasonic technology is used in various industrial applications. One of these applications is ultrasonic plastic welding. A high-power ultrasonic transducer is used as a mechanical vibrations source in this method. Generally, the vibration amplitude at the output surface of transducers is approximately 10-20 microns [1]. In order to weld plastics, the amplitude of vibration should be increased to provide the required energies. Boosters and horns do this amplification. In order to optimize the energy transfer, the natural frequency of the booster and horn must be near the resonant frequency of the transducer [2]. There are some essential requirements like nodal plan located on the booster, magnification factor, and longitudinal resonant frequency of components, dimensions, and materials properties that should be considered in the design of components [3]. Also, some external parameters have a significant effect on the efficiency and performance of the system. For example, external force and workpieces' stiffness are

some of those parameters that their effect has not been investigated analytically so far. Studies show that the design, optimization, and analysis of these components are done thoroughly by finite element software like ANSYS and COMSOL, which requires several times for trials and error. Wang et al. [4] designed an optimized horn using FEM for the high amplitude of vibrations. Kumar et al. [5] optimized the location of grooves on the body of block horns by the genetic algorithm to obtain uniform output amplitude. Wei et al. [6] designed a stepped horn using the differential equation of wave in one dimension. The 1D method has low accuracy; therefore, they designed the horn using trial and error in the COMSOL software. Naseri et al. [7] studied a horn for a metal forming process. They experimentally changed the length of the horn in order to tune it for forming metal billets in a mold and reducing forming forces. The system's resonant frequency is directly related to the stiffness of workpieces, but they did not study it. Rosca [2] designed a horn and considered the stiffness of the workpiece using the 1D equation. The external forces and the stiffness significantly affect the quality of welding. Bae et al. [8] designed a horn for polymer sheet forming. They experimentally surveyed the effect of external forces on the quality of forming and temperature changing in the workpiece. Shuyu [9] calculated the resonant frequency using coupled vibrations of a transducer. He presented an approximate analytical method and surveyed the effect of geometrical dimensions on the resonant frequency. The electrical behavior of a transducer depends on boundary conditions like mechanical loads, temperature, etc. By modeling the transducer as an equivalent RLC circuit, its behavior can be investigated under different conditions. Kauczor et al. [10, 11] investigated the frequency response of a high-power ultrasonic transducer utilizing its RLC equivalent circuit. Also, the mechanical quality factor of the transducer can be calculated by this model. Boontaklang and Chompoo-Inwai [12] used an equivalent RLC circuit model to propose a novel tracking and tuning technique for an ultrasonic transducer. They clearly explained a way of calculating the frequency response of an RLC model (e.g., admittance circle, phase, and amplitude diagram). Shuyu et al. [13] studied a tubular high-power composite ultrasonic transducer that generates radial and longitudinal waves. He modeled the transducer as an RLC circuit and calculated its resonant frequency. Moreover, he illustrated the theoretical relationship between the resonant frequency and geometrical dimensions.

In this paper, the effect of the workpiece's stiffness and material properties on the frequency response of an ultrasonic transducer is investigated by an analytical model. A precise mathematical model based on the coupling of longitudinal and radial vibrations is made to calculate the frequency response, resonant and anti-resonant frequency, mode shape, and magnifying factor of vibrations under different working conditions. First, the analytical model of a transducer, booster, horn, and workpiece are presented. After that, the system is simulated with FEM software to verify the analytical model. Finally, the components are fabricated for experimental tests and verifications.

2. Analytical Modeling

An ultrasonic transducer is usually made up of three types of material: steel, titanium, and Piezoelectric. The booster and horn are usually made up of Aluminum 7075-T6. Every component is modeled as solid or hollow cylinders or exponential parts in this paper. By writing the dynamic equilibrium for stresses on a cylindrical 3D element (Figure 1).

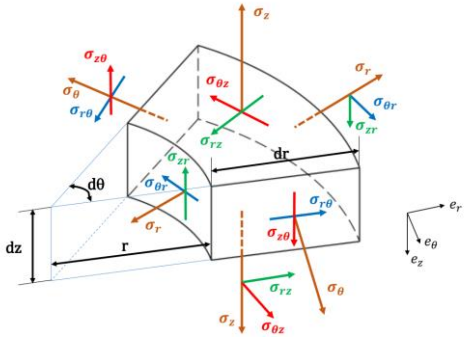

Fig. 1. Cylindrical element of components

Ignoring the shear stresses, the equation of motion in the longitudinal direction is as follows.

$$\frac{\partial^2 u_z}{\partial z^2} + k_z{}^2 u_z = 0 \tag{1}$$

Which k_z is apparent wave number and is defined as:

$$k_z = \frac{\omega}{V_z} \tag{2}$$

Where ω is the angular frequency, V_z is the apparent speed of the wave, which is defined as:

$$V_z = \sqrt{\frac{E_z}{\rho}} \tag{3}$$

Where ρ is density, E_z is the apparent modulus of elasticity defined as follows.

$$E_z = \frac{E}{1 - \frac{\nu}{n}} \tag{4}$$

Where E is the real young modulus, ν is the Poisson ratio, and the mechanical coupling coefficient, n, is defined as the ratio of longitudinal stress to lateral stress consisting of radial and circumferential stresses.

$$n = \frac{\sigma_z}{\sigma_r + \sigma_\theta} \tag{5}$$

By solving the differential equation of motion (Eq.1), longitudinal displacement relation in a cylinder is obtained as:

$$\boldsymbol{u_z(z) = A\,cos(k_z Z) + B\,sin(k_z Z)} \tag{6}$$

Also, longitudinal displacement relation in exponential parts is:

$$\boldsymbol{u_z(z) = e^{-\beta Z}\ \left(A'\,cos\left(\left[\sqrt{k_z^2 - \beta^2}\ \right] z\ \right) + B'\,sin\left(\left[\sqrt{k_z^2 - \beta^2}\ \right] z\ \right)\right)} \tag{7}$$

A, B, A', and B' are unknown coefficients in the above equations. The radial displacement differential equation and its answer are as follows.

$$\boldsymbol{\frac{\partial^2 u_r}{\partial r^2} + \frac{1}{r}\frac{\partial u_r}{\partial r} + \left({k_r}^2 - \frac{1}{r^2}\right) u_r = 0\ \rightarrow\ u_r(r) = CJ_0(k_r r) + DY_0(k_r r)} \tag{8}$$

Radial frequency equations for hollow and solid cylinders are obtained by applying the radial boundary conditions. Radial forces at a hollow cylinder's internal and external radius are zero. The two boundary conditions yield the following frequency equation [14].

$$\boldsymbol{\frac{k_r a J_0(k_r a) - \frac{(1-\nu-2\nu n)}{(1-\nu n)} J_1(k_r a)}{k_r b J_0(k_r b) - \frac{(1-\nu-2\nu n)}{(1-\nu n)} J_1(k_r b)} = \frac{k_r a Y_0(k_r a) - \frac{(1-\nu-2\nu n)}{(1-\nu n)} Y_1(k_r a)}{k_r b Y_0(k_r b) - \frac{(1-\nu-2\nu n)}{(1-\nu n)} Y_1(k_r b)}} \tag{9}$$

The radial force at the outer radius of a solid cylinder is zero, and radial displacement in the center of the cylinder is zero. The two boundary conditions yield the following frequency equation.

$$\boldsymbol{a k_r J_0(k_r a) - \left[\frac{(1-\nu-2\nu n)}{(1-\nu n)}\right] J_1(k_r a) = 0} \tag{10}$$

Structural damping of components is taken into account using an imaginary young's modules as follows.

$$\boldsymbol{\widetilde{E} = E + E' i = E(1 + \eta i)} \tag{11}$$

Where $\boldsymbol{E}$ is the real young modulus, $\boldsymbol{E'}$ is loss modulus and $\eta = \frac{E'}{E}$ is the structural loss factor. Also, the dielectric loss of piezoelectrics is defined as a complex electric permittivity coefficient.

$$\boldsymbol{\widetilde{\epsilon}_{33}\ = \epsilon_{33}(1 + (\tan\delta) i)} \tag{12}$$

Where ϵ_{33} is the real electric permittivity along 'Z' direction and $\tan\delta$ is the loss factor. The following assumptions are taken into account for the analytical model:

1) The vibration mode does not change in the wave propagation along with the components.
2) Wave reflection is discarded at contact surfaces.

3) Shear stresses and strains are ignored.
4) The waves inside the parts are assumed sinusoidal.
5) The diameter change in the components is far from the critical values, so the effect of chamfers and fillets is ignored.
6) The acoustic impedance of air is ignored, so the horn or booster that works in the air is called "unloaded," and its stress is considered zero.
7) The machined surfaces for the wrench seat on the booster and horn are disregarded.
8) Torsional and bending modes are ignored.
9) Set screws that connect components are ignored.
10) Differential equations in the radial and longitudinal directions are considered.
11) To drive the radial frequency equation of exponential segments, the mean radius of these segments is considered.
12) The threaded part of the matching component is considered a solid cylinder.
13) The piezoelectrics and copper electrodes are considered as integrated components.
14) Slip and friction between contact surfaces are ignored.

Figure 2 shows the vibrating system. The system is divided into 16 segments, including hollow and solid cylinders and exponential parts. The workpiece is considered as a spring that is attached to the output surface of the horn. The spring stiffness is related to the workpiece's young module, thickness, and contact area. Also, the external force is applied to the booster's flange, and its reaction is on the output surface of the horn.

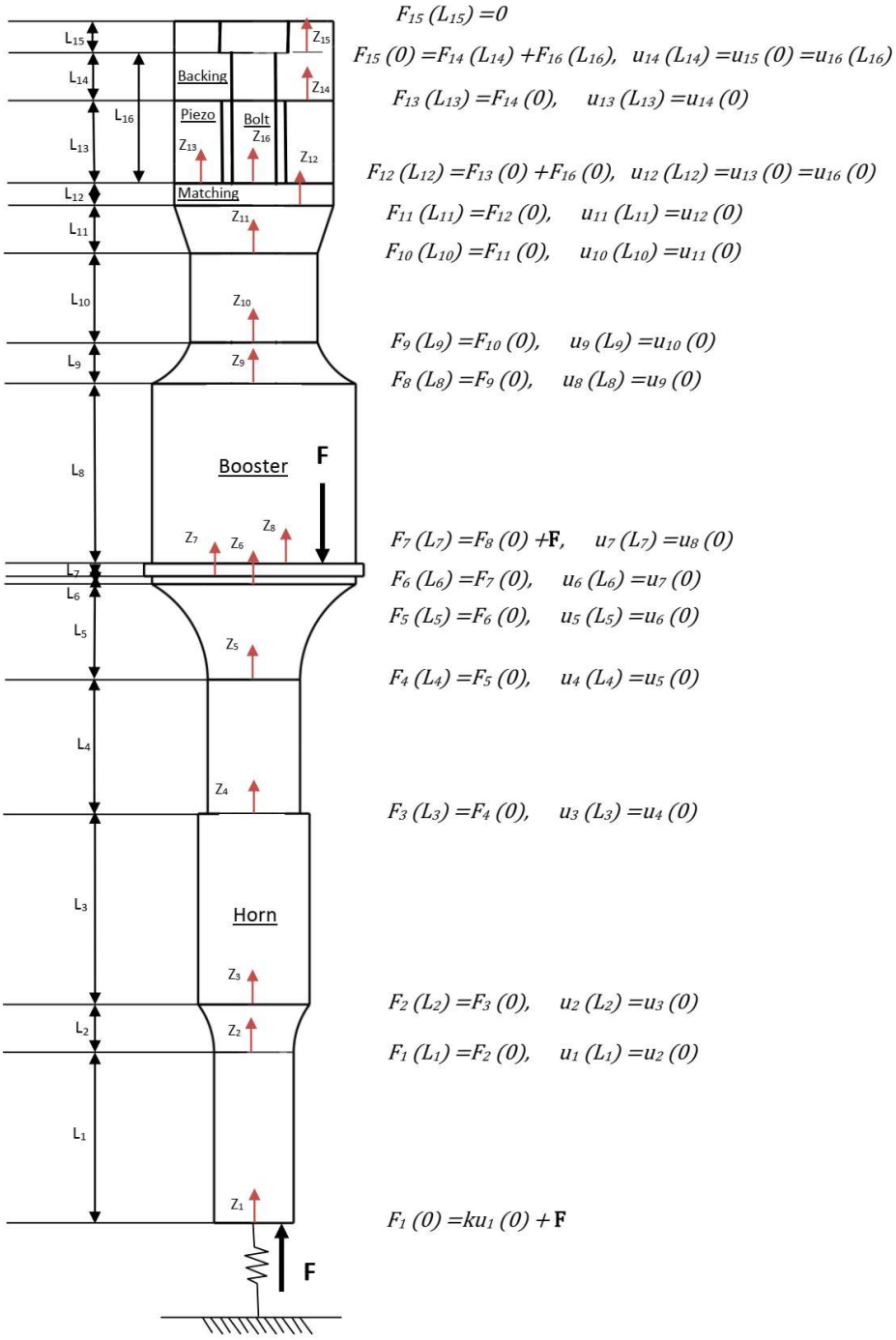

Fig.2 the vibrating system and boundary conditions

The longitudinal displacement relations for each element are as follows.

$$\boldsymbol{u_1(z_1) = A\cos(k_1 z_1) + B\sin(k_1 z_1)} \tag{13}$$

$$u_2(z_2) = e^{-\beta_1 Z_2}\left(C\cos\left(\left[\sqrt{k_2^2-\beta_1^2}\right]z_2\right)+D\sin\left(\left[\sqrt{k_2^2-\beta_1^2}\right]z_2\right)\right) \quad (14)$$

$$u_3(z_3) = E\cos(k_3 z_3) + F\sin(k_3 z_3) \quad (15)$$

$$u_4(z_4) = G\cos(k_4 z_4) + H\sin(k_4 z_4) \quad (16)$$

$$u_5(z_5) = e^{-\beta_2 Z_5}\left(I\cos\left(\left[\sqrt{k_5^2-\beta_2^2}\right]z_5\right)+J\sin\left(\left[\sqrt{k_5^2-\beta_2^2}\right]z_5\right)\right) \quad (17)$$

$$u_6(z_6) = K\cos(k_6 z_6) + L\sin(k_6 z_6) \quad (18)$$

$$u_7(z_7) = M\cos(k_7 z_7) + N\sin(k_7 z_7) \quad (19)$$

$$u_8(z_8) = O\cos(k_8 z_8) + P\sin(k_8 z_8) \quad (20)$$

$$u_9(z_9) = e^{\beta_3 Z_9}\left(Q\cos\left(\left[\sqrt{k_9^2-\beta_3^2}\right]z_9\right)+R\sin\left(\left[\sqrt{k_9^2-\beta_3^2}\right]z_9\right)\right) \quad (21)$$

$$u_{10}(z_{10}) = S\cos(k_{10} z_{10}) + T\sin(k_{10} z_{10}) \quad (22)$$

$$u_{11}(z_{11}) = e^{-\beta_4 Z_{11}}\left(U\cos\left(\left[\sqrt{k_{11}^2-\beta_4^2}\right]z_{11}\right)+V\sin\left(\left[\sqrt{k_{11}^2-\beta_4^2}\right]z_{11}\right)\right) \quad (23)$$

$$u_{12}(z_{12}) = W\cos(k_{12} z_{12}) + X\sin(k_{12} z_{12}) \quad (24)$$

$$u_{13}(z_{13}) = Y\cos(k_{13} z_{13}) + Z\sin(k_{13} z_{13}) \quad (25)$$

$$u_{14}(z_{14}) = A'\cos(k_{14} z_{14}) + B'\sin(k_{14} z_{14}) \quad (26)$$

$$u_{15}(z_{15}) = C' \cos(k_{15} z_{15}) + D' \sin(k_{15} z_{15}) \tag{27}$$

$$u_{16}(z_{16}) = E' \cos(k_{16} z_{16}) + F' \sin(k_{16} z_{16}) \tag{28}$$

The stiffness of the workpiece is defined as:

$$k_w = \frac{A_w E_w}{L_w} \tag{29}$$

In this equation, A_w, E_w and L_w are the contact area, young's module, and thickness of the workpiece, respectively. In this paper a polyethylene workpiece with 0.1 GPa Young's modulus and 2 mm thickness is used. Table 1 shows the dimensions of the vibrating system.

Table1. Dimensions of the vibrating system

Element Number	Length (mm)	Inner Radius (mm)	Outer Radius (mm)	Material
1	53.7	-	12.5	Al
2	15	-	17.5	Al
3	60	-	17.5	Al
4	45.2	-	14.5	Al
5	30	-	14.5	Al
6	2.5	-	32	Al
7	4	-	34.5	Al
8	56.5	-	32	Al
9	13	-	20	Al
10	28	-	20	Ti
11	15	-	20	Ti
12	7	-	25	Ti
13	26	10	25	PZT-4
14	15	7	25	St
15	10	11	25	St
16	41	-	7	St

Using the boundary conditions and without an exciting electrical field, the following matrix equation is obtained to calculate the longitudinal resonant frequency. (The complete matrix equation is given in the appendix).

$$\begin{bmatrix} \boldsymbol{The\ coefficients} \\ \boldsymbol{matrix} \end{bmatrix} \begin{bmatrix} \boldsymbol{A} \\ \boldsymbol{B} \\ \vdots \\ \boldsymbol{E'} \\ \boldsymbol{F'} \end{bmatrix} = \begin{bmatrix} \mathbf{F} \\ \mathbf{0} \\ \vdots \\ \mathbf{F} \\ \mathbf{0} \\ \vdots \\ \mathbf{0} \end{bmatrix} \tag{30}$$

F is the external force that is placed in the constant matrix. The determinant of the coefficients matrix should be equal to zero to obtain the longitudinal frequency equation. So, external forces are not considered in modal analysis. They do not affect natural frequencies.

Table 2 shows the mechanical properties of the components.

Table2. Mechanical properties of the components

Material	Density (Kg/m³)	Young's Modulus (GPa)	Poisson's ratio	Damping ratio
Al 7075-T6	2923	69	0.33	0.0005 [15]
Steel 304	7917	200.57	0.28	0.00041
Titanium	4499	112.05	0.32	0.00192 [16]

Table 3 shows the physical properties of piezoelectric.

Table3. PZT-4 characteristics

Characteristic	Symbol	Unit	Amount
Elastic constants	s_{11}^{E}	1/Pa	16.5e-12
	s_{12}^{E}	1/Pa	-4.78e-12
	s_{13}^{E}	1/Pa	-8.45e-12
	s_{33}^{E}	1/Pa	19.5e-12
Permittivity	ε_{11}^{T}	1	1475
	ε_{22}^{T}	1	1475
	ε_{33}^{T}	1	2700
Constants	d_{31}	C/N	-0.4e-10
	d_{33}	C/N	1e-10
Density	ρ	Kg/m³	7800
Damping ratio	η	1	0.009
Loss factor	$tan\ \delta$	1	0.00132

By solving the system of equations which includes one longitudinal and 16 radial frequency equations, the resonant frequency of the vibrating set and each element's mechanical coupling coefficient are calculated and shown in table 4.

Table4. Solution of the system of equations

Third Longitudinal Resonant Frequency	19208 Hz
n_1	-65.72
n_2	-44.64
n_3	-32.55
n_4	-47.37

n_5	-17.98
n_6	-8.04
n_7	-7.66
n_8	-8.98
n_9	-13.94
n_{10}	-24.98
n_{11}	-18.36
n_{12}	-14.67
n_{13}	-2.55
n_{14}	-15.45
n_{15}	-13.42
n_{16}	-2.43

In the next step, the results obtained from solving the system of equations are used for forced vibration analysis of the transducer and its frequency response. For this purpose, an electrical field is considered on the piezoelectric.

The electro-mechanical equation of piezoelectric rings can be expressed as follows [17].

$$\{\boldsymbol{S}\} = [\boldsymbol{s^E}]\{\boldsymbol{T}\} + [\boldsymbol{d}]^{\boldsymbol{t}}\{\boldsymbol{E}\} \tag{31}$$

$$\{\boldsymbol{D}\} = [\boldsymbol{d}]\{\boldsymbol{T}\} + [\boldsymbol{\epsilon^T}]\{\boldsymbol{E}\} \tag{32}$$

Where $\{S\}$ is the mechanical strain vector and $\{D\}$ is the electric charge density vector. Using piezoelectric equations, the electric field is entered into the matrix equation [16]. Rows 26th and 28th of the constant matrix have electric field terms. By solving the new matrix equation, frequency response, mode shape, and displacement amplitude are calculated, and the effect of workpiece stiffness is investigated. Electrical admittances related to radial and longitudinal vibrations is obtained from the following equations [16].

$$\boldsymbol{Y_{31}} = \frac{\boldsymbol{I_{31}}}{\boldsymbol{V_3}} = -\frac{\boldsymbol{2\pi\omega}}{\boldsymbol{l}}\left[\left(\frac{\boldsymbol{d_{31}+nd_{33}}}{\boldsymbol{s_{11}^E+s_{12}^E+2ns_{13}^E}}\right)\left\{\frac{\boldsymbol{(s_{11}^E-s_{12}^E)2d_{31}}}{\boldsymbol{j(a)y(b)-y(a)j(b)}}\left[\boldsymbol{\big(y(b)-y(a)\big)\big(aJ_1(k_ra)-bJ_1(k_rb)\big)}\right.\right.\right. \tag{33}$$
$$\left.\left.\left.\boldsymbol{+\big(j(a)-j(b)\big)\big(aY_1(k_ra)-bY_1(k_rb)\big)}\right]\boldsymbol{-d_{31}(a^2-b^2)}\right\}+\boldsymbol{\epsilon_{33}^T}\left(\frac{\boldsymbol{a^2}}{\boldsymbol{2}}-\frac{\boldsymbol{b^2}}{\boldsymbol{2}}\right)\right]\boldsymbol{tan(\omega t)}\times\boldsymbol{N_p}$$

$$\boldsymbol{Y_{33}} = \frac{\boldsymbol{I_{33}}}{\boldsymbol{V_3}} = \frac{\boldsymbol{-\pi\omega(a^2-b^2)}}{\boldsymbol{l}}\left\{\left(\frac{\boldsymbol{d_{31}}}{\boldsymbol{n}}+\boldsymbol{d_{33}}\right)\boldsymbol{E_z}\left[-\frac{\boldsymbol{Yk_z}}{\boldsymbol{E_3}}\boldsymbol{\sin(k_zz)}+\frac{\boldsymbol{Zk_z}}{\boldsymbol{E_3}}\boldsymbol{\cos(k_zz)}-\boldsymbol{d_{33}}\right]+\boldsymbol{\epsilon_{33}^T}\right\}\times\boldsymbol{N_p}\times\boldsymbol{\tan(\omega t)} \tag{34}$$

l is the total length of piezoelectrics, N_P is the number of piezoelectric rings, I_{31} and I_{33} are currents due to radial and longitudinal vibrations, respectively, and V_3 is the applied voltage to the piezoelectric.

The overall current and admittance of the system are calculated as follows.

$$\boldsymbol{I_3} = \boldsymbol{I_{31}} + \boldsymbol{I_{33}} \tag{35}$$

$$Y_3 = Y_{31} + Y_{33} \tag{36}$$

Figure 3 shows the Nyquist diagram of admittance of the transducer, plotted by the analytical model under loaded and free conditions. The Radius of the diagram decreases once the stiffness of the workpiece increases.

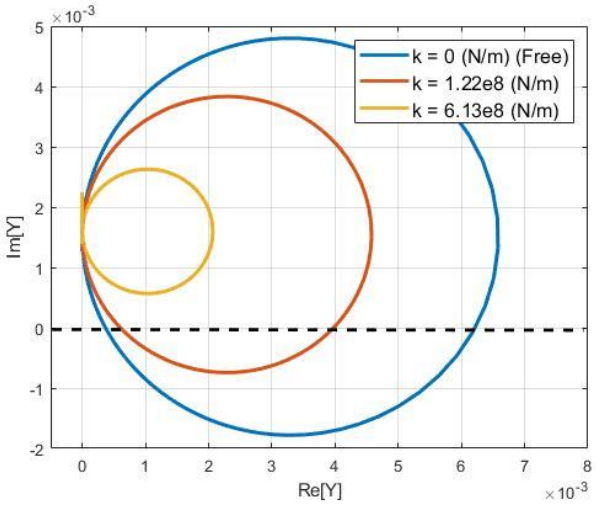

Fig3. The Nyquist diagram of the transducer's admittance under free and loaded condition

Figure 4 indicates that as the stiffness of the workpiece increases, the resonant frequency increases, and both displacement and admittance amplitude decrease.

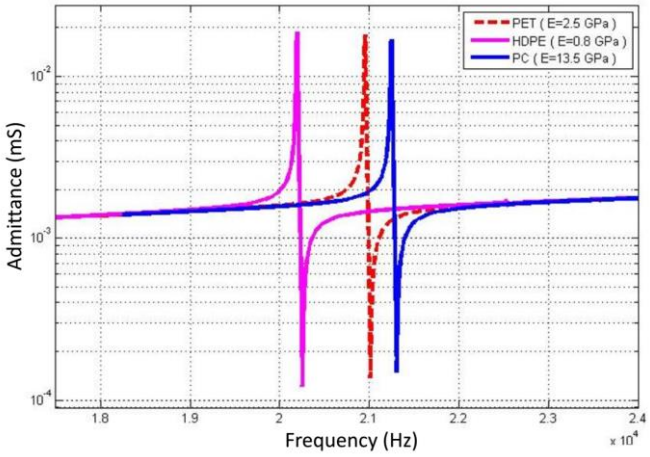

(a)

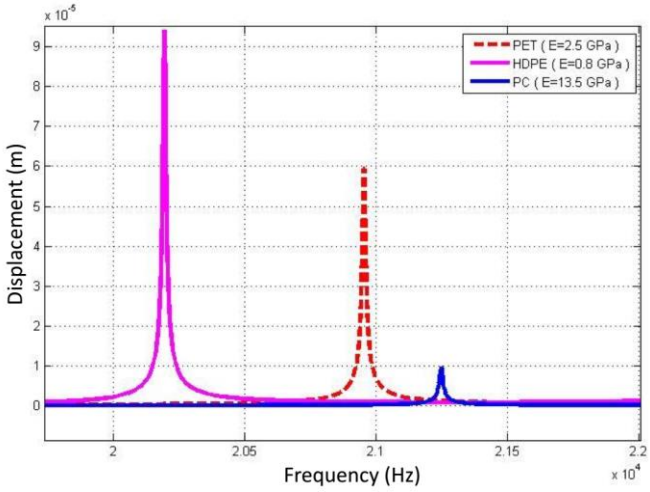

(b)

Fig4. (a) Frequency response of the transducer (b) Displacement amplitude of the output surface of horn in contact with different workpieces at 300V

Figure 5 shows the effect of voltage on the displacement amplitude of the output surface of the horn at free conditions. As the voltage increases, the displacement increases.

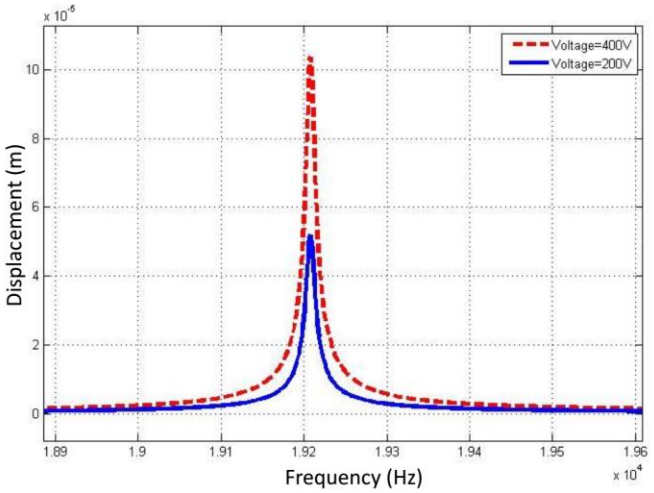

Fig.5 The effect of voltage on the displacement

Figure 6 shows the effect of changing density (or mass of the system), Young's modulus, and damping of Aluminum components in the continuum model on the mechanical quality factor.

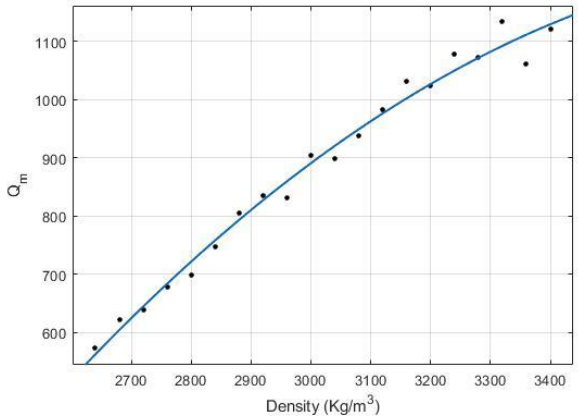

(a)

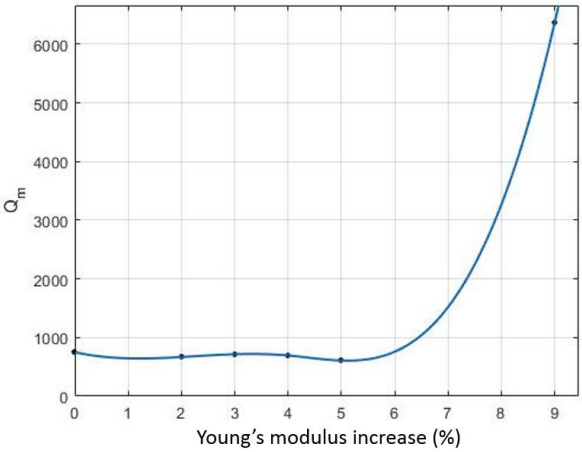

(b)

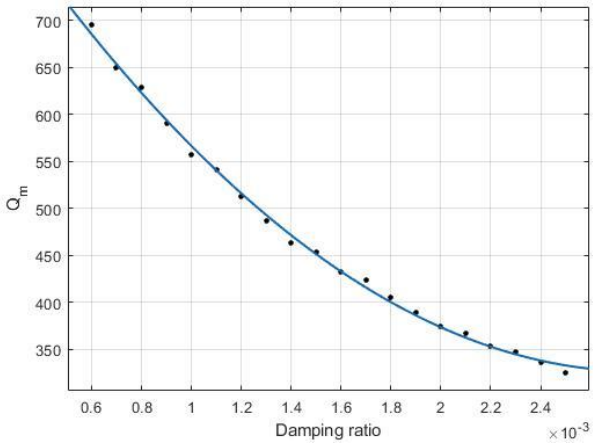

(c)

Fig.6 The effect of (a) density, (b) Young's modulus, and (c) damping of Aluminum components on the mechanical quality factor using the continuum model

The mechanical quality factor for the transducer with specifications presented in the paper is calculated 750 using the continuum model. The amount of the Q factor increases by increasing the density of Aluminum components.

Figure 7 (a) shows that in the large value of the damping, the admittance phase is totally positive. Figure 7 (b) shows the Nyquist diagram of admittance and the effect of damping on the radius of the circle.

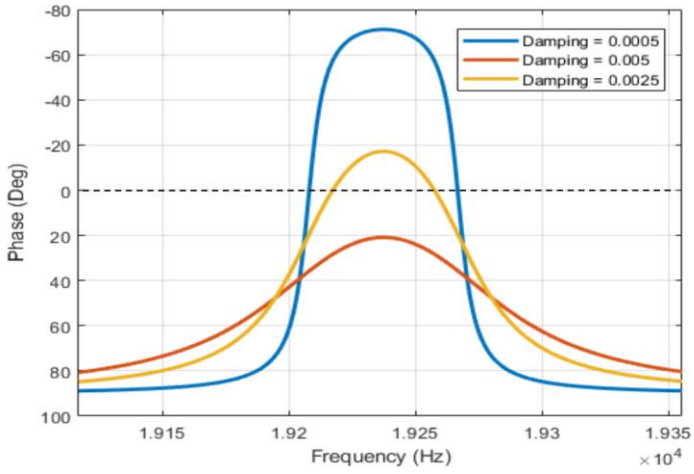

(a)

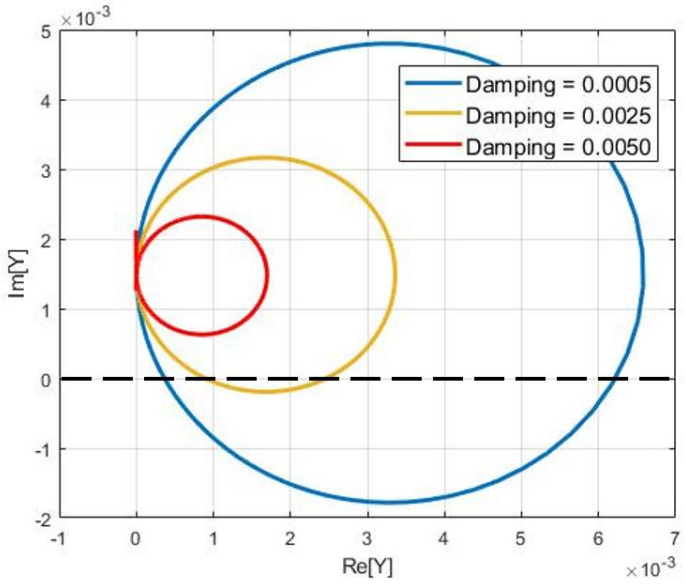

(b)

Fig.7 (a) The effect of changing Damping on the admittance phase in the continuum model (b) damping effect on the Nyquist diagram.

3. Numerical Modeling

ANSYS software is used for numerical analyses. First, the vibrating system is modeled in CATIA software with the exact dimensions and materials in the analytical model. Next, it is imported into the ANSYS software for modal analysis. The resonant frequency is obtained under free conditions and in contact with a workpiece. Also, the mode shape of the system is computed. Figure 8 shows meshes of components for a 3D simulation. The mesh type is Explicit, and the number of nodes is 6841.

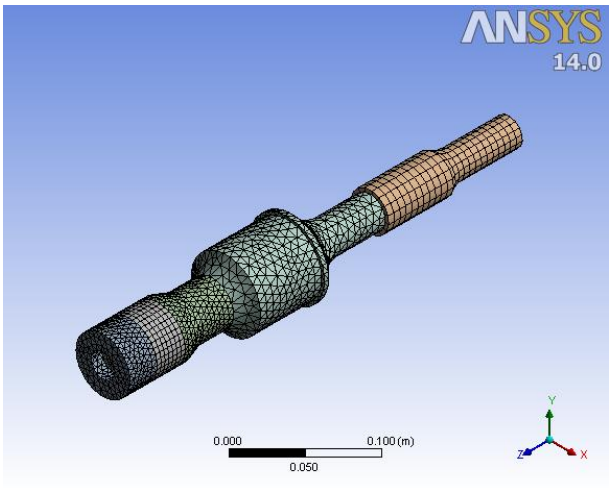

Fig.8 Meshed model of the vibrational system

The obtained results from the modal analysis show that the resonant frequency of the vibrating system under free conditions is 19280 Hz which has a 0.3% error with the analytical model (19208 Hz). Figure 9 shows the modal analysis result while the system encounters a workpiece with a Young modulus of 0.1 GPa.

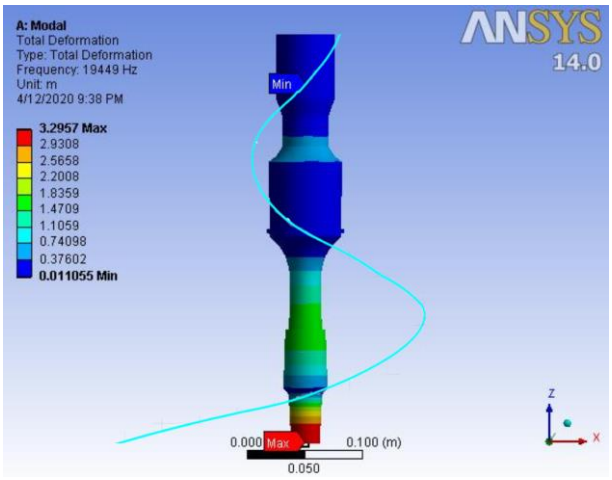

Fig.9 Third longitudinal mode shape at the frequency of 19449 Hz

Figure 10shows that resonant frequency in both models increases by increasing the young's modulus of the workpiece.

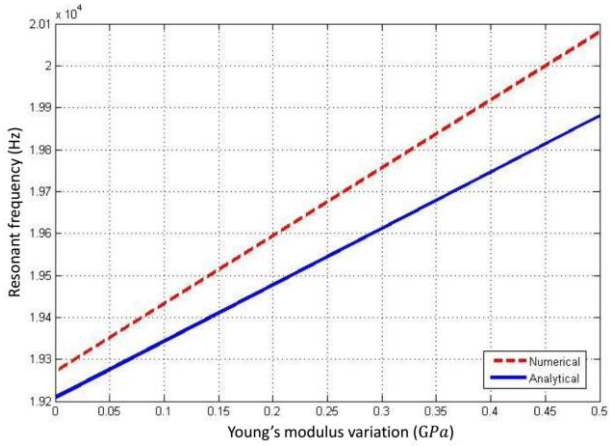

Fig.10 The effect of workpiece young's modulus on the resonant frequency

Also, the mode shape of the vibrating system is obtained by the developed analytical model at 300V and compared with the numerical model's result under free conditions. As figure 11 shows, there are three nodal planes on the system. Booster's nodal plane is important to be on the flange, avoiding transfer of vibrations to welding machine structures. Moreover, the magnification factor of each component can be calculated by this figure.

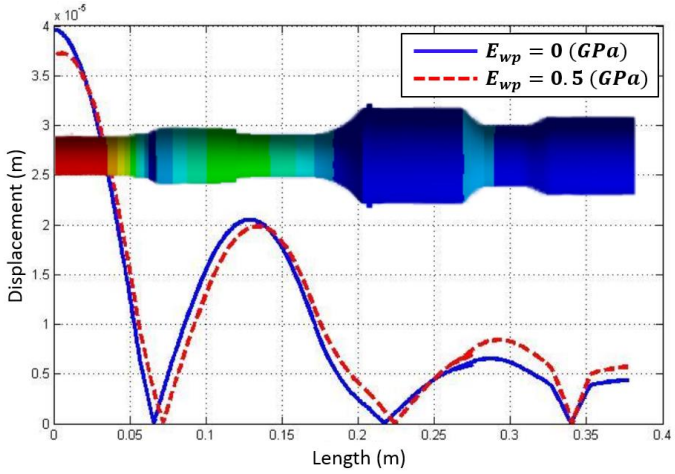

Fig.11 Theoretical mode shape in two different young's modulus of the workpiece

4. Fabrication and experimental tests

All the components are fabricated and assembled according to table 1 dimensions for experimental verifications. Moreover, a fixture is designed to hold the vibrating system from the booster's nodal plane and attach it to the body of the machine (Figure 12).

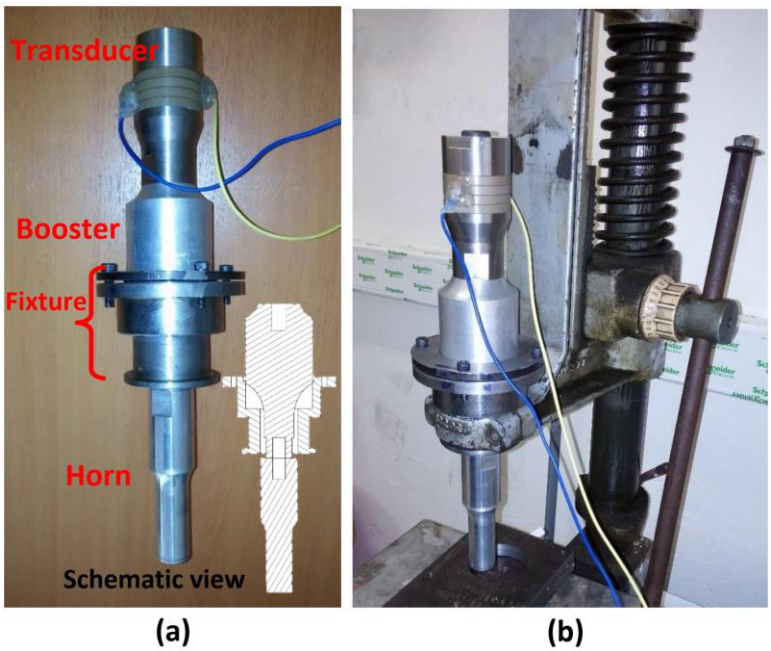

Fig.12 (a) The vibrating system and fixture (b) Column of a welding machine

The system's resonant frequency is measured by an ultrasonic power supply (ULPS 2000, Alfa. Co, Iran). Fig.13 shows experimental tests of the frequency response of the system. As shown in figure 13 (c), the resonant frequency of the system is measured 19200 Hz at 300V under free conditions, which has 0.04% error with analytical result (19208 Hz) and 0.4% error with the numerical result (19280 Hz). When the vibrating system is encountered with a workpiece figure 13 (d), the resonant frequency increases to 19270 Hz. Also, increasing the voltage, reduces the resonant frequency due to decreasing the piezoelectric Young's modulus figure 13 (b). Generally, resonant frequency increases in the experiments by increasing the external force. According to Eq.29, when external force increases, the thickness of the workpiece decrease, and it causes the increase of the stiffness of spring. So, the resonant frequency increases.

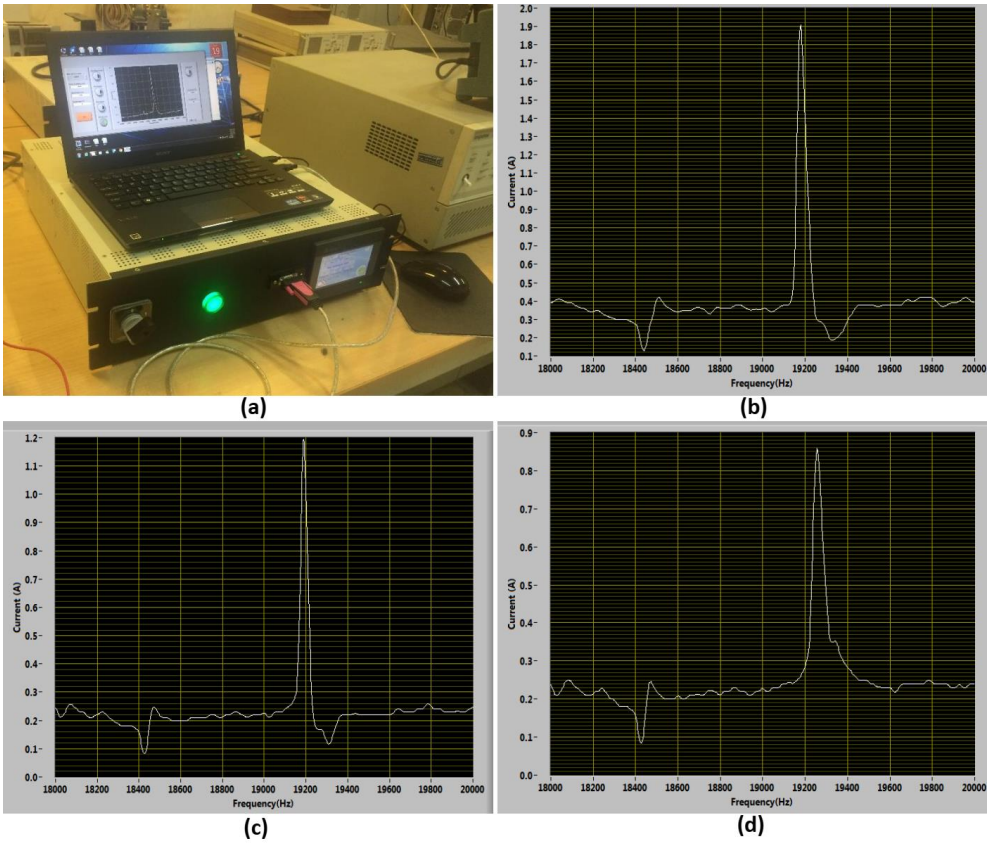

Fig.13 (a) Ultrasonic power supply (b) Resonant frequency at 500V under free condition (19180 Hz) (c) Resonant frequency at 300V under free condition (19200 Hz) (d) Resonant frequency at 300V with the workpiece (19270 Hz)

In order to measure the admittance's frequency response, an LCR meter (LCR-8110G, GW INSTEC, Taiwan) is used. Figure 14 shows the experimental setup to measure the admittance of the vibrating system.

Fig.14 The admittance measurement of the vibrating system with LCR meter

The result of this test is compared with the analytical model in figure 15. The admittance in resonant and anti-resonant frequencies are compared with the analytical results in table 5.

Table5. Experimental Vs. analytical results

Parameter	Experimental	Analytical	Error (%)
Resonant frequency (Hz)	19203	19208	0.02
Anti-resonant frequency (Hz)	19270	19265	0.02
Admittance in resonant (mS)	0.0176	0.01755	0.2
Admittance in anti-resonant (mS)	0.000138	0.0001182	14.34

The admittance phase is calculated by the analytical model and compared with the experimental results in figure 16.

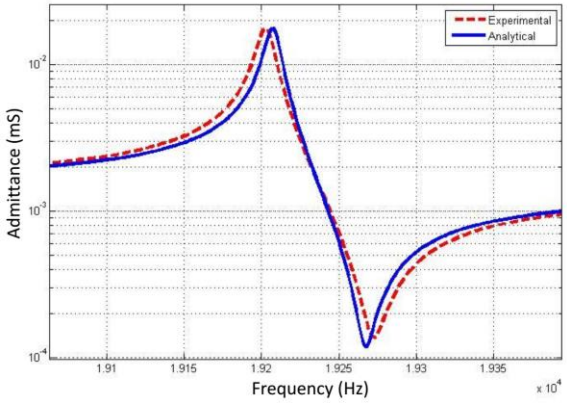

Fig.15 Amplitude of the frequency response of the admittance

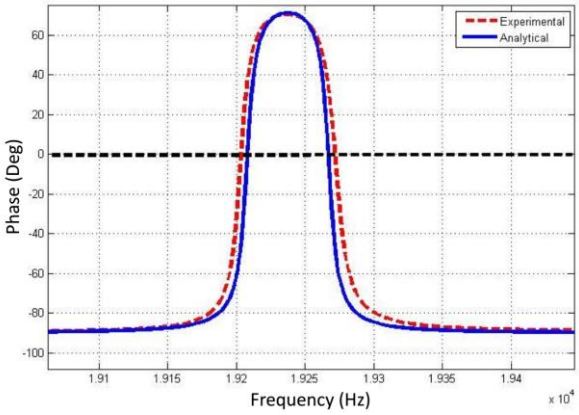

Fig.16 Phase of the frequency response of the admittance

To measure the amplitude of displacement of the horn's output surface, a gap sensor (AEC-5509, Applied electronics, Japan) is used. Figure 17 shows the test and its results.

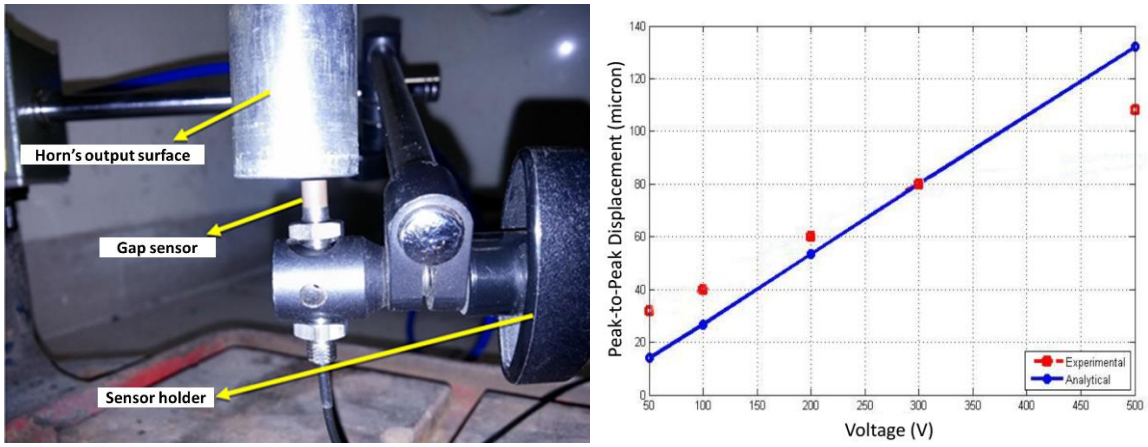

Fig.17 Displacement measurement of the horn at different voltages

According to the graph, the displacement is increased by increasing the voltage in both experimental and analytical results. The average error is about 23.6%.

5. Conclusions

A new analytical model was developed, and its accuracy was examined by comparing its results with an RLC equivalent circuit, numerical model, and experimental tests. The proposed analytical model showed excellent results in calculating the resonant frequency, and mode shape in contact with workpieces. Also, it had good predictions of resonant and anti-resonant frequency. On the other hand, the effect of the parameters like damping, stiffness, and mass are investigated by an RLC equivalent circuit and the analytical model. However, there is an inevitable random error in measuring some parameters, such as the amplitude of the vibration. However, the analytical model results showed a good agreement with the results of the experiments. Simplifications of the analytical model, such as ignoring the reflection of waves in contact surfaces, can be sources of errors in the results of calculating the admittance and the amplitude of vibrations. The effect of changing voltage on the physical properties of piezoceramics is our future researches.

6. Competing Interests

We declare that we have no significant competing financial, professional, or personal interests that might have influenced the performance or presentation of the work described in this manuscript.

7. Availability of data and materials

Raw data were generated at Metrology and Advanced Mechatronics Laboratory, faculty of mechanical engineering, Tarbiat Modares University, Tehran, IRAN. Derived data supporting the findings of this study are available from the corresponding author on request.

8. Authors contributions

Amir yazdian: Conceived the analysis, collected the data, contributed data or analysis tools, performed the analysis, wrote the paper.

Mohammad reza karafi: Developed the analytical model, check the results, contribute in experiments, organized, and revised the paper.

9. Ethical Approval

Irrelevant to the paper.

10. Consent to Participate

Irrelevant to the paper

References

[1] M.R. Karafi, S.A. Mirshabani, An Analytical Approach to Design of Ultrasonic Transducers Considering Lateral Vibrations, Journal of Stress Analysis 3 (2) (2019) 47-58.

[2] Ioan-Calin Rosca, Mihail-Ioan Pop, Nicolae Cretu, Experimental and numerical study on an ultrasonic horn with shape designed with an optimization algorithm, Applied Acoustics 95 (2015) 60-69.

[3] PLLM Derks, The design of ultrasonic resonators with wide output cross-sections, Technische Hogeschool Eindhoven, 1984.

[4] D.-A. Wang, W.-Y. Chuang, K. Hsu, H.-T. Pham, Design of a Bézier-profile horn for high displacement amplification, Ultrasonics 51 (2) (2011) 148-156.

[5] R. Dipin Kumar, M. Roopa Rani, S. Elangovan, Design and Analysis of Slotted Horn for Ultrasonic Plastic Welding, Applied Mechanics and Materials 592–594 (2014) 859–63.

[6] Zongsu Wei, James A. Kosterman, Ruiyang Xiao, Gim-Yang Pee, Meiqiang Cai, Linda K. Weavers, Designing and characterizing a multi-stepped ultrasonic horn for enhanced sonochemical performance, Ultrasonics Sonochemistry 27 (2015) 325-333.

[7] R. Naseri, K. Koohkan, M. Ebrahim, F. Djavanroodi, H. Ahmadian, Horn design for ultrasonic vibration-aided equal channel angular pressing, Int J Adv Manuf Technol 90 (2017) 1727–1734.

[8] Hojin Bae, Keun Park, Design and analysis of ultrasonic horn for polymer sheet forming, Int. J. of Precis. Eng. and Manuf.-Green Tech. 3 (2016) 49–54.

[9] Lin Shuyu, Analysis of the sandwich piezoelectric ultrasonic transducer in coupled vibration, The Journal of the Acoustical Society of America 117 (2005) 653-661.

[10] C. Kauczor, T. Schulte, N. Fröhleke, Resonant power converter for ultrasonic piezoelectric converter, 8th International Conference on New Actuators, Bremen, Germany, 2002.

[11] C. Kauczor, N. Fröhleke, Inverter Topologies for Ultrasonic Piezoelectric Transducers with High Mechanical Q-Factor, IEEE 35th Annual Power Electronics Specialists Conference (IEEE Cat. No.04CH37551), 2004, pp. 2736-2741 Vol.4, doi: 10.1109/PESC.2004.1355265.

[12] Suttipong Boontaklang, Chow Chompoo-Inwai, Automatic Resonance-Frequency Tuning and Tracking Technique for a 1MHz Ultrasonic-Piezoelectric-Transducer Driving Circuit in Medical Therapeutic Applications Using dsPIC Microcontroller and PLL Techniques, International Journal of Intelligent Engineering and Systems 12(6) (2019) 14-24.

[13] Shuyu Lin, Long Xu, Wenxu Hu, A new type of high power composite ultrasonic transducer, Journal of Sound and Vibration 330 (7) (2011) 1419-1431.

[14] S. Lin, Coupled vibration of isotropic metal hollow cylinders with large geometrical dimensions, J. Sound Vib. 305 (2007) 308–316.

[15] Amir Abdullah, Massoud Malaki, On the damping of ultrasonic transducers' components, Aerospace Science and Technology 28 (1) (2013) 31-39.

[16] Mohammadreza Karafi, Sobhan Kamali, A continuum electro-mechanical model of ultrasonic Langevin transducers to study its frequency response, Applied Mathematical Modelling 92 (2021) 44-62.

[17] S.Y. Lin, Coupled vibration analysis of piezoelectric ceramic disk resonators, J. Sound Vib. 218 (1998) 205–217.

Supplementary Files

This is a list of supplementary files associated with this preprint. Click to download.

- Appendixsupplimentaymaterials.docx